SETAC PRESS

Environmental Toxicology and Chemistry, Vol. 33, No. 5, pp. 1035–1042, 2014

Printed in the USA

INFLUENCE OF CARBON AND METAL OXIDE NANOMATERIALS ON AQUEOUS CONCENTRATIONS OF THE MUNITION CONSTITUENTS CYCLOTRIMETHYLENETRINITRAMINE (RDX) AND TUNGSTEN

JONATHON A. BRAME,†‡ ALAN J. KENNEDY,† CHRISTOPHER D. LOUNDS,§ ANTHONY J. BEDNAR,† PEDRO J.J. ALVAREZ,‡ ANDREA M. SCOTT,† and JACOB K. STANLEY*†

†US Army Engineer Research and Development Center, Environmental Laboratory, Vicksburg, Mississippi, USA
‡Rice University, Houston, Texas, USA
§Badger Technical Services, Vicksburg, Mississippi, USA

(Submitted 15 November 2013; Returned for Revision 28 December 2013; Accepted 18 January 2014)

Abstract: There is an increasing likelihood of interactions between nanomaterials and munitions constituents in the environment resulting from the use of nanomaterials as additives to energetic formulations and potential contact in waste streams from production facilities and runoff from training ranges. The purpose of the present research was to determine the ability of nano-aluminum oxide (Al_2O_3) and multiwalled carbon nanotubes (MWCNTs) to adsorb the munitions constituents cyclotrimethylenetrinitramine (RDX) and tungsten (W) from aqueous solution as a first step in determining the long-term exposure, transport, and bioavailability implications of such interactions. The results indicate significant adsorption of RDX by MWCNTs and of W by nano-Al_2O_3 (but not between W and MWCNT or RDX and nano-Al_2O_3). Kinetic sorption and desorption investigations indicated that the most sorption occurs nearly instantaneously (<5 min), with a relatively slower, secondary binding leading to statistically significant but relatively smaller increases in adsorption over 30 d. The RDX sorption that occurred during the initial interaction was irreversible, with long-term, reversible sorption likely the result of a secondary interaction; as interaction time increased, however, the portion of W irreversibly sorbed onto nano-Al_2O_3 also increased. The present study shows that strong interactions between some munitions constituents and nanomaterials following environmental release are likely. Time-dependent binding has implications for the bioavailability, migration, transport, and fate of munitions constituents in the environment. *Environ Toxicol Chem* 2014;33:1035–1042. © 2014 SETAC

Keywords: Nanomaterial Environmental fate Munitions constituent Military Adsorption

INTRODUCTION

Nanomaterials are increasingly used to improve the performance of current and future military technologies, in addition to their rapidly increasing use in industrial and commercial applications. For example, nano-aluminum and multiwalled carbon nanotubes (MWCNTs) are incorporated into nanothermites, energetics, and propellant formulations [1–3]. Other applications include the use of graphene and MWCNTs in composites, enhanced fabrics, sensors, batteries, antennas, and energetic formulations [1,4–6].

While the fate and effects of contaminants of military concern (e.g., energetic compounds and metal munitions constituents) have received thorough study, less is known about how the ultimate environmental fate of these constituents may be affected by the incorporation of nanomaterials into military technologies. Some nanomaterials may affect the migration of toxic chemicals in the environment because of their large surface area, crystalline structure, and reactivity [7,8]. These traits can increase contaminant sorption [9–20], which can facilitate or retard transport of the contaminant in the environment [21]. Although they could have significant impacts on the environmental fate of munitions constituent materials, the effects of these interactions on the environmental fate of energetics have not been examined, with the exception of a degradation compound of trinitrotoluene (2,4-dinitrotoluene) as part of a larger study on sorption of polar and nonpolar organics to MWCNTs [22]. With advances in nanomaterial applications in the military, particularly in energetics and explosives [1,23,24], there is a great need to better understand these interactions and their potential effects on fate and transport in the environment [21].

The present study addressed the propensity of select nanomaterials used in munitions formulations or other military technologies (MWCNTs and nano-aluminum oxide [Al_2O_3]) to bind to military-relevant contaminants in aqueous systems to assess potential implications on environmental fate. To this end, sorption extent, kinetics, mechanism, strength, and reversibility were determined. The compounds cyclotrimethylenetrinitramine (RDX) and tungsten (W) were selected as a military-relevant model organic and metal, respectively. We used kinetic adsorption and desorption tests and adsorption isotherms to help determine the type, extent, and potential environmental impact of these interactions.

MATERIALS AND METHODS

Source of particles and munitions constituents

Multiwalled carbon nanotubes, hydroxylated MWCNTs (MWCNT-OH; 1.76% hydroxylated by weight), and graphene nanoplatelets were obtained from Cheap Tubes. Nano-Al_2O_3 was obtained from Nanostructured & Amorphous Materials. As an additional comparison, a bulk Al_2O_3 material (Sigma-Aldrich; supplier-specified 50–200 μm) was tested. Military-grade RDX was obtained from the Holston Army Ammunition Plant and used as received. Tungsten was reagent-grade sodium tungstate ($Na_2WO_4 \cdot 2H_2O$, 99% purity), obtained from Sigma-Aldrich.

* Address correspondence to jacob.k.stanley@us.army.mil.
Published online 27 January 2014 in Wiley Online Library (wileyonlinelibrary.com).
DOI: 10.1002/etc.2531

Particle characterization

Nanoparticles were submitted to Virginia Polytechnic Institute and State University (Blacksburg, VA, USA) for imaging via transmission electron microscopy (TEM) using a Philips model 420T (FEI) TEM in bright-field mode at 100 kV. Particle size was determined from these TEM images using Image Pro Plus (Media Cybernetics) image analysis software. Surface area of particles was determined using a Nova 3200e BET (Brunauer, Emmett, and Teller) surface area analyzer (Quantachrome Instruments). Further details on the characterization of the 11-nm and bulk Al_2O_3 [25,26] and the MWCNTs [27–29] used in the present study can be found in previously published studies by our group. Briefly, the nano-Al_2O_3 and bulk Al_2O_3 particle sizes ranged from 4 nm to 12 nm (after sonication) and 50 μm to 200 μm, respectively. The MWCNT and MWCNT-OH had outer diameter ranges of 10 nm to 30 nm and 20 nm to 30 nm, respectively. Lengths of both MWCNTs ranged from 10 000 nm to 30 000 nm.

Batch sorption studies

Initial batch sorption studies consisted of the following munitions constituent and nanoparticle pairings: nano-Al_2O_3 and RDX, MWCNT and RDX, nano-Al_2O_3 and W, and MWCNT and W. We then explored other nanoparticles (functionalized MWCNTs, graphene, bulk Al_2O_3) with similar structures and properties based on those results for comparison. Munitions constituent concentrations in the sorption studies were nominally 2 mg/L, and nanoparticle concentrations were nominally 500 mg/L. The munitions constituent solutions were created using moderately hard reconstituted water (MHRW) made according to US Environmental Protection Agency (USEPA) [30] specifications. Prior to interaction, stock suspensions of nanomaterials were probe-sonicated (Branson Sonifier 450) for 5 min at 40% power and duty cycle, then bath-sonicated (Branson 8510) for 24 h. Stock solutions of RDX and W were created and allowed to stir for 24 h prior to initiation of the sorption study. Sorption experiments were performed in 150-mL silanized glass Erlenmeyer flasks in triplicate. Munitions constituents and nanomaterials were allowed to interact while stirring on a multiposition magnetic stir plate for a period of 7 d to determine the propensity for binding of munitions constituents to nanomaterials in aqueous solutions.

At the end of the 7-d interaction period, a 2-mL sample was taken from the flask and centrifuged at 5000 *g* for 60 min (Beckman J6; Beckman-Coulter). Comparison with ultracentrifugation at 100 000 *g* (60 min) showed no significant difference in measured munitions constituent concentrations in the supernatant between the 2 centrifugation methods (data not shown); thus, the 5000 *g* centrifugation was acceptable for removing the nanomaterials from solution. The munitions constituent concentration of the supernatant was then quantified to assess the amount of sorption to the nanomaterials over the 7-d sorption test. Kinetic studies were performed similarly, with interaction periods ranging from 0 d to 36 d.

Isotherm fitting

To elucidate binding mechanisms and better understand their influence on long-term sorption and possible biological interactions, we performed isotherm tests for both the RDX–MWCNT and W–nano-Al_2O_3 interactions. Adsorption was measured as described above with an initial sorption mixing period of 7 d. After comparing the data to several different isotherm models, including Freundlich, Dubinin-Polanyi, and multilayer models, the isotherm data were fit using a Langmuir model [31]

$$q = \frac{q_{\max} \times b \times C_e}{1 + b \times C_e} \quad (1)$$

In this model, q is the mass loading (mg munitions constituent/g nanoparticle), C_e is the equilibrium sorbent concentration (mg/L), $q_{\max}$ is the maximum loading value (mg munitions constituent/g nanoparticle), and b is the Langmuir constant (L/mg). The Langmuir model assumes a finite number of adsorption sites on the adsorbing material, resulting in a monolayer of sorbent coverage, which corresponds to the maximum loading capacity, $q_{\max}$. At low sorbent concentrations, the mass loading onto the adsorbent is linear with respect to the equilibrium sorbent concentration in solution, while it approaches a maximum loading value as a result of complete surface coverage at high sorbent concentrations. The data were fit to the Langmuir equation using a nonlinear least-squares approach.

Desorption testing

To measure the strength of the sorption interactions, desorption experiments were conducted in which the nanomaterials were resuspended in clean MHRW after an initial sorption period, and the amount of munitions constituent desorbed during this rinsing was measured. Initial sorption periods were 1 d and 21 d to observe differences between short-term and long-term sorption on the binding strength during desorption. Following resuspension, samples were taken after various time intervals of vigorous stirring (0 d, 1 d, 3 d, 7 d, and 14 d) to determine the amount of munitions constituent desorbed as a function of time mixing in clean MHRW. All experiments were performed in triplicate.

Analytical quantitation

Concentrations of RDX were determined using an Agilent 1100 Series high-performance liquid chromatograph (HPLC) equipped with a Supelco RP-amide C-16 column and a photodiode array detector using a flow rate of 1 mL/min and a detection wavelength at 230 nm. Methanol and water (55:45) were used as the mobile phase solvents with a column temperature of 45 °C.

Aqueous W concentrations were determined using inductively coupled plasma atomic emission spectroscopy (ICP-AES) or inductively coupled plasma mass spectrometry (ICP-MS), depending on the concentration, following modifications of USEPA methods 6010 and 6020. Briefly, W metal was quantitated using the 207.912-nm emission line or *m/z* 182 ion with confirmation using the 224.876-nm emission line and *m/z* 183 ion using ICP-AES and ICP-MS, respectively. Instruments were calibrated using National Institute of Standards and Technology traceable commercially available standards and calibration verification using the National Institute of Standards and Technology traceable second source standards. Scandium and yttrium were added online using a mixing-T as internal standards to correct for instrumental drift during ICP-AES analysis, whereas terbium and holmium were added to correct for drift during ICP-MS analyses. Measured W metal concentrations were assumed to exist as WO_4^{2-} in solution [12] but reported as milligrams of W.

RESULTS

Particle characterization

Table 1 shows the particle size and surface area characterization data for the nanomaterials used in the present study.

Table 1. Nanomaterial size and surface area[a]

Material	Nominal particle size (nm)	Measured particle size (nm)	BET surface area (m^2/g)
Nano Al_2O_3	11	21.5 ± 8.9	218.9 ± 7.3
Bulk Al_2O_3	50 000–200 000	1300 ± 800	145.2 ± 11.0
MWCNT	20 (width)	21.3 ± 4.6 (width)	126.9 ± 2.3
MWCNT-OH	13–18	22.2 ± 3.9	138.7 ± 8.5
Graphene	$<2 \times 10^3$	1700 ± 1400	8.6 ± 2.5

[a]Multiwalled carbon nanotube length was nominally 10 000 nm to 30 000 nm (Kennedy et al. [28]).
BET = Brunauer, Emmett, and Teller; MWCNT = multiwalled carbon nanotube; MWCNT-OH = hydroxylated multiwalled carbon nanotube.

Measured primary particle sizes (from TEM images) generally approximated nominal or manufacturer-reported ranges, though measured nano-Al_2O_3 particles were slightly larger than expected and the bulk Al_2O_3, while still micron-scale, was smaller than the reported nominal particle size. The nano-Al_2O_3 particles had the largest mass normalized surface area, followed by the bulk Al_2O_3 particles, MWCNT, and MWCT-OH. The surface area of graphene was substantially less than that of the other materials tested.

Aqueous sorption studies

Munitions constituent sorption to various nanoparticles (mass of munitions constituent/mass of nanoparticle) is shown in Figure 1. The RDX sorption was limited on nano-Al_2O_3 but more prominent on MWCNT; therefore, functionalized MWCNTs and graphene nanoparticles were also tested, with the largest sorption on the nonfunctionalized MWCNTs. Sorption of W was most pronounced on nano-Al_2O_3, with much less adsorption onto MWCNTs. Bulk Al_2O_3 sorption was also tested and showed one-third the sorption of nano-Al_2O_3 (Figure 1). When normalized by surface area, nano-Al_2O_3 sorption was still 2 times that of bulk Al_2O_3.

Isotherms

The data for both RDX–MWCNT and W–nano-Al_2O_3 interactions followed a Langmuir-type adsorption profile in which the munitions constituent loading was linear at low equilibrium munitions constituent concentrations and approached a maximum at high concentrations. The slope in the linear portion of the W–nano-Al_2O_3 sorption isotherm was significantly higher than that in the RDX–MWCNT isotherm. Both data sets were fit to the Langmuir equation (Figure 2), and the resulting maximum loadings and Langmuir constants from these fits are shown in Table 2.

Kinetics

The initial loading (<5 min mixing) of RDX onto MWCNTs was 70% of the final loading at 36 d (1.6 mg RDX/g MWCNT vs 2.3 mg RDX/g MWCNT, respectively) with $t = 21$ d, 28 d, and 35 d statistically higher than $t = 0$ d, 4 d, 7 d, and 14 d and with a generally increasing trend throughout the experiment (Figure 3a). The initial loading (<5 min mixing) of W onto nano-Al_2O_3 was 50% of the maximum loading, which occurred at 14 d (0.8 mg W/g nano-Al_2O_3 vs 1.6 mg W/g nano-Al_2O_3, respectively; Figure 3b). The fractional loading reached 80% (1.2 mg W/g nano-Al_2O_3) after stirring for 1 d and increased to equilibrium at 14 d. The loading of W on nano-Al_2O_3 at 21 d of mixing was not statistically higher than any of the loading measurements from day 1 on, indicating an apparent steady state (Figure 3b).

Desorption

The RDX–MWCNT loading (mass of RDX adsorbed per gram MWCNT) after 1 d of sorption was 1.7 mg RDX/g MWCNT, which decreased to 1.4 mg RDX/g MWCNT on resuspension in clean MHRW. During 14 d of mixing in clean MHRW after this

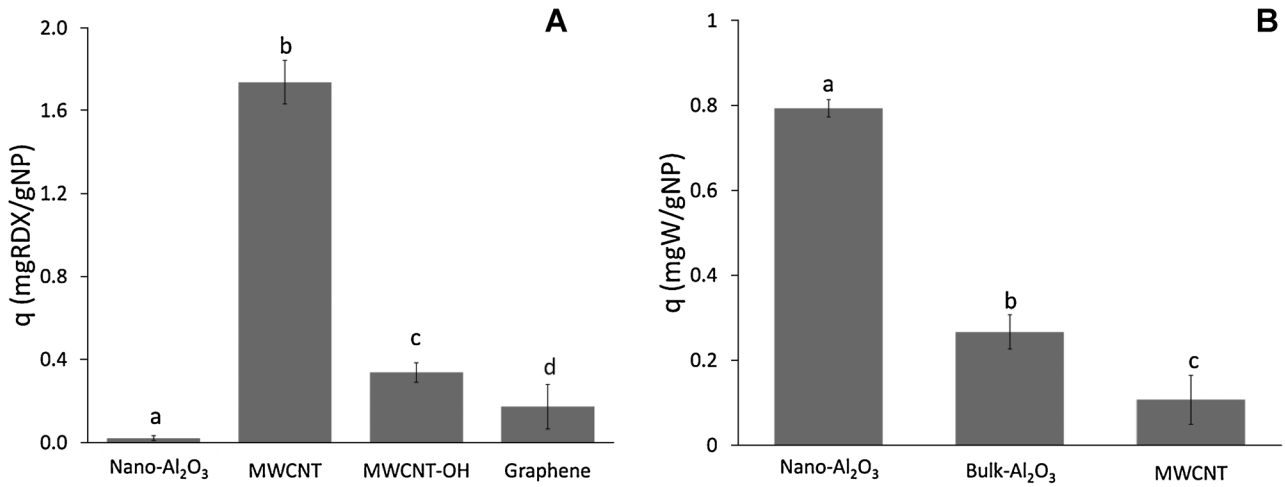

Figure 1. Sorption loading of RDX onto nano-Al_2O_3, MWCNT, MWCNT-OH, and graphene (**A**) and W onto nano-Al_2O_3, bulk Al_2O_3, and MWCNTs (**B**) after a 7-d interaction period; RDX had the strongest interaction with MWCNTs, wheresas W had the strongest interaction with nano-Al_2O_3. Lowercase letters (a, b, c, d) indicate data points that are statistically different from each other. Error bars represent 1 standard deviation from the mean. $[RDX]_0$, $[W]_0 = 2$ mg/L. q = mass loading; RDX = cyclotrimethylenetrinitramine; W = tungsten; MWCNT = multiwalled carbon nanotube; MWCNT-OH = hydroxylated MWCNT; NP = nanoparticle.

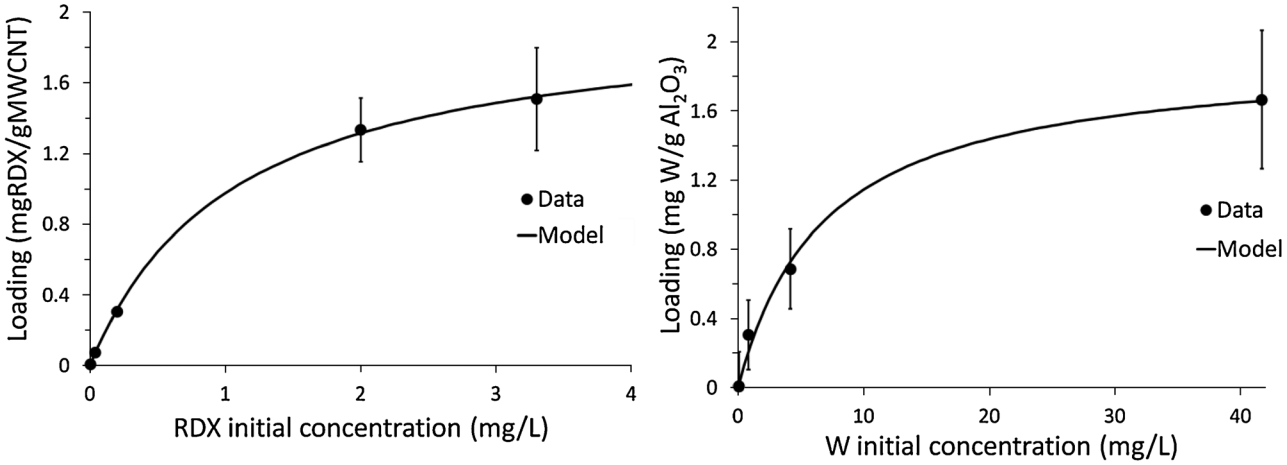

Figure 2. Isotherm data for RDX–MWCNT and W–nano-Al_2O_3 interactions showing munitions constituent loading as a function of initial munitions constituent concentration. The data were fit using the Langmuir isotherm equation with $q_{max,RDX} = 2.0 \pm 0.1$ mg RDX/g MWCNT and $b_{RDX} = 1.1 \pm 0.1$ L/mg; $q_{max,W} = 1.9 \pm 0.1$ mg W/g nano-Al_2O_3 and $b_W = 0.1 \pm 0.05$ L/mg. [MWCNT], [nano-Al_2O_3] = 500 mg/L. Error bars represent 1 standard deviation from the mean. RDX = cyclotrimethylenetrinitramine; W = tungsten; MWCNT = multiwalled carbon nanotube; W = tungsten.

Table 2. Langmuir constants modeled from isotherm data

Munitions constituent–nanoparticle sorption pair	q_{max} (maximum loading value)	b (Langmuir constant)
RDX–MWCNT	2.0 ± 0.1 mg RDX/g MWCNT	1.1 ± 0.1 L/mg RDX
W–nano-Al_2O_3	1.9 ± 0.1 mg W/g nano-Al_2O_3	0.1 ± 0.05 L/mg W

RDX = cyclotrimethylenetrinitramine; MWCNT = multiwalled carbon nanotube; W = tungsten.

initial rinsing, the RDX loading did not change significantly. The RDX–MWCNT loading after 21 d of initial sorption was higher, at 1.9 mg RDX/g MWCNT, but this loading also decreased to 1.4 mg RDX/g MWCNT on resuspension in clean MHRW. During an additional 14 d of mixing in clean MHRW, the RDX loading increased slightly to 1.5 mg RDX/g MWCNT as some of the RDX that was initially desorbed when resuspended in clean MHRW was adsorbed back onto the MWCNTs (Figure 4a).

After 1 d of sorption, W–nano-Al_2O_3 loading was 0.9 mg W/g nano-Al_2O_3, which decreased to 0.6 mg W/g nano-Al_2O_3 on resuspension in clean MHRW. During 14 d of mixing in clean MHRW after the initial rinsing, the W loading decreased to 0.3 mg W/g nano-Al_2O_3 by day 7 as a result of desorption and remained relatively constant through day 14. The W–nano-Al_2O_3 loading after 21 d of sorption was 1.9 mg W/g nano-Al_2O_3, which decreased to 1.7 mg W/g nano-Al_2O_3 on resuspension in clean MHRW. During 14 d of additional mixing in clean MHRW, the W loading decreased to 1.4 mg W/g nano-Al_2O_3 by day 7 as a result of desorption and remained relatively constant through day 14 (Figure 4b).

DISCUSSION

From Figure 1 it is apparent that the adsorption of some munitions constituents is stronger to certain nanomaterials (e.g., RDX with MWCNTs, W with nano-Al_2O_3), whereas other combinations produce little or no interaction (e.g., RDX with nano-Al_2O_3 or graphene, W with MWCNTs). For those

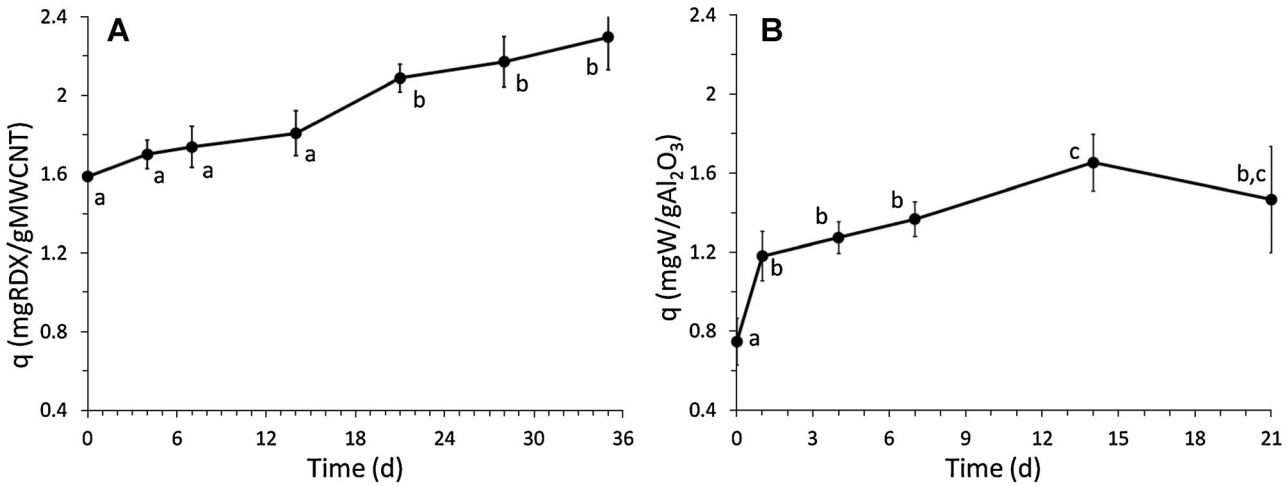

Figure 3. Mass loading (q) of RDX onto MWCNTs (**A**) and W onto nano-Al_2O_3 (**B**) with time. $[RDX]_0$, $[W]_0 = 2$ mg/L; [MWCNT], [nano-Al_2O_3] = 500 mg/L. Lowercase letters (a, b, c) indicate groups of data points that are statistically different from each other. Error bars represent 1 standard deviation from the mean. RDX = cyclotrimethylenetrinitramine; W = tungsten; MWCNT = multiwalled carbon nanotube.

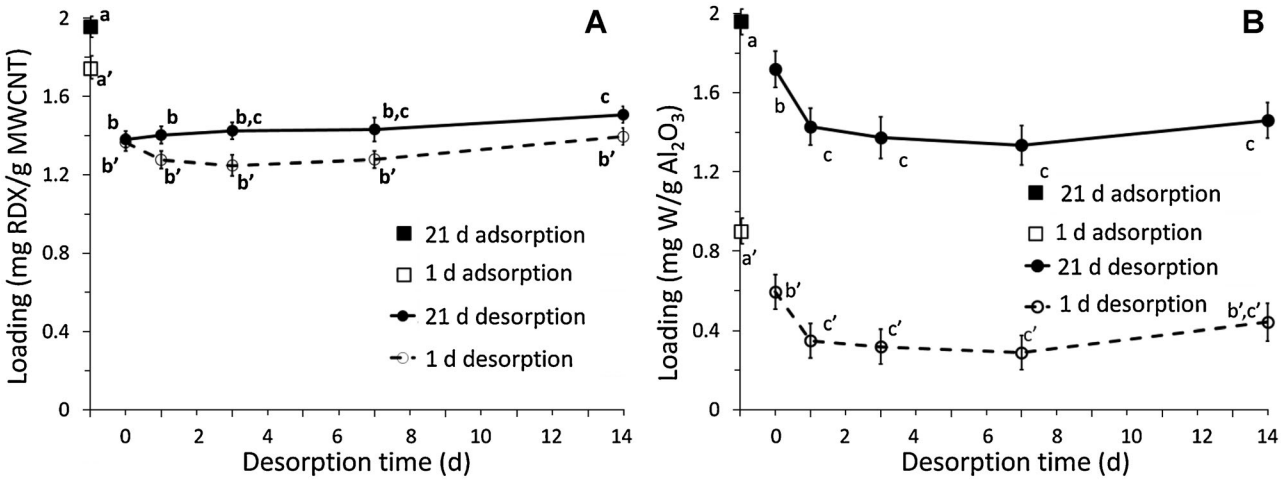

Figure 4. Desorption data for RDX–MWCNT (**A**) and W–nano-Al_2O_3 (**B**) interactions. Munitions constituents were mixed with nanomaterials for either 1 d or 21 d to allow adsorption, then rinsed and mixed with clean moderately hard reconstituted water to measure desorption over time. $[RDX]_0$, $[W]_0 = 2$ mg/L; [MWCNT], [nano-Al_2O_3] = 500 mg/L. Lowercase letters (a, b, c, a′, b′, c′) indicate groups of data points that are statistically different from each other. Error bars represent 1 standard deviation from the mean. RDX = cyclotrimethylenetrinitramine; W = tungsten; MWCNT = multiwalled carbon nanotube.

combinations with little or no interaction, the nanomaterials will likely not alter the fate and transport of the munitions constituent, and both the nanomaterial and the munitions constituent will follow traditional fate and transport models, many of which have been studied extensively for these materials [32–34]. However, for those materials that interact strongly with each other, the fate, transport, and bioavailability will be altered by their interactions. The mechanism, strength, kinetics, and reversibility of the sorption reactions can influence whether these interactions will increase or decrease impact on the environment and receptor organisms. Therefore, to help elucidate these processes the majority of the present study focuses on those interactions with the highest sorption: RDX with MWCNTs and W with nano-Al_2O_3.

Isotherms

The Langmuir isotherm model provided a strong fit ($r^2 > 0.98$) to both the RDX–MWCNT and the W–nano-Al_2O_3 initial sorption data (Figure 2 and Table 2) compared with alternative models (multilayer, Freundlich, and Dubinin-Polanyi adsorption isotherms), which did not adequately fit the data ($r^2 < 0.6$). Langmuir isotherm behavior indicates that the initial sorption interactions occur at specific adsorption sites on the nanomaterial surface up to a monolayer of coverage. Within the tested concentration range, we observed both a linear sorption pattern (at low munitions constituent concentrations) and the approach to complete surface coverage (at high munitions constituent concentrations). The approach toward an asymptotic maximum loading strongly suggests that adsorption sites were saturated at higher concentrations, consistent with the Langmuir isotherm model.

In locations where munitions constituents and nanomaterials are co-located, the nanomaterials could act as an effective sink at low munitions constituent concentrations (<0.1 mg/L RDX, <1 mg/L W), removing the munitions constituents through sorption and decreasing their bioavailability and mobility in the environment. At high munitions constituent concentrations, however, the nanomaterials' sorption sites could become saturated and bioavailability and mobility would depend on the munitions constituent's traditional fate and transport models.

Sorption mechanisms

There are several potential sorption mechanisms that may explain the observed RDX–MWCNT interactions. The π electrons in the MWCNT material can contribute to sorption through n-π electron donor–acceptor interactions, and Lewis acid–base binding could also account for sorption of electron-accepting sorbents. Hydrophobicity was previously shown to correlate poorly with nanotube adsorption [22,35], and because RDX is slightly hydrophilic (log octanol/water partition coefficient = 0.68) and was shown to interact weakly with organic compounds in soil sorption experiments [36], hydrophobic sorption is unlikely. Chen et al. [22] found that nitro groups increased the sorption affinity of organic contaminants to carbon nanotubes because of the π-electron polarizability of the nanotubes and that more nitro groups produced stronger interactions (see also Schwarzenbach et al. [31]). Additionally, the nitrogen atoms in the RDX ring contribute a strong electronegativity and add unbound n-electrons, which can contribute to the n-π electron donor–acceptor attraction. It is also possible that this electron transfer could reduce the RDX [37], although no reduced RDX by-products, such as hexahydro-1-nitroso-3,5-dinitro-1,3,5-triazine (MNX), hexahydro-1,3-dinitroso-5-nitro-1,3,5-triazine (DNX), or hexahydro-1,3,5-trinitroso-1,3,5-triazine (TNX) were observed by HPLC analysis.

The decreased sorption of RDX onto oxidized MWCNTs (Figure 1), in which the OH surface groups withdraw π electrons from the surface of the nanotube, is consistent with the postulated n-π electron donor–acceptor sorption mechanism [38,39]. Coughlin and Ezra [39] proposed that the O functional groups withdraw π electrons from graphitic surfaces, leading to weaker interactions between the adsorbate and adsorbent. The presence of O functionalities on the MWCNTs could also decrease sorption as a result of steric constraints, preventing RDX penetration into micropore spaces, decreased sorption sites caused by the presence of hydroxyl groups [38], or preferential sorption of water molecules because of H-bonds with O functionalities on the carbon surface [40–42].

The significantly higher sorption onto MWCNTs than graphene is likely a result of graphene's smaller surface area. The measured surface area of the graphene was much smaller

than that of the MWCNTs (Table 1), with fewer sorption sites and reduced overall sorption capacity. When normalized for surface area, RDX sorption by graphene was only slightly lower than sorption by MWCNTs (data not shown). If the sorption mechanism is similar, it may be assumed that the resulting environmental implications of RDX–graphene interactions are similar to those of RDX–MWCNT interactions. For the purposes of the present study, however, we focused on a mass normalization representing a comparable quantity of various materials that could potentially be released into the environment; therefore, our analysis centers on RDX–MWCNT interactions.

Since W in environmental matrices (including MHRW in the present study) almost exclusively exists as tungstate ion (WO_4^{2-}) [12], the sorption mechanism of W onto nano-Al_2O_3 is likely a result of the electrostatic interaction between the tungstate anions and charged metal oxides in solution [43–45]. Although this process can be highly dependent on the pH of the solution [46], these experiments were conducted at circumneutral pH in MHRW to simulate environmental conditions.

Kinetics

Both W–nano-Al_2O_3 and RDX–MWCNT interactions exhibit a significant initial loading of the munitions constituent onto the nanomaterial, followed by a slower increase in loading with time (Figure 3). The initial loading ($t = 0$) took place very rapidly as the munitions constituents and nanomaterials were mixed together briefly and then almost immediately (<5 min) removed for analysis. The observed time-dependent sorption has been reported previously for many organic contaminants such as chlorinated solvents, pesticides, and polycyclic aromatic hydrocarbons [47].

The initial loading of RDX onto MWCNTs was about 70% of the final loading after 36 d, with a generally increasing trend throughout the experiment (Figure 3a). Many organic chemicals have slow sorption behavior that accounts for anywhere from 30% to 90% of the total loading over timescales of 1 mo to several months. Pignatello and Xing [47] suggest that this is likely the result of mass transfer limitations or activation energy barriers. Slow sorption of organics binding to natural particles and sediments is often attributed to diffusion limitations caused by a heterogeneous pore-size distribution. Because this system involves pure MWCNTs, which have a more homogeneous distribution of pore sizes than soil or sediments [48], the long-term increase in sorption is more likely a result of bonds with higher activation energies that require longer equilibrium times, such as internal sorption sites [38] or secondary interactions such as RDX–RDX interactions between aqueous and sorbed RDX molecules [49].

Interestingly, the RDX loading during the kinetics tests reached values higher than the maximum surface loading predicted by the Langmuir model: 2.3 mg RDX/g MWCNT after 36 d (Figure 3) compared with 2.0 mg RDX/g MWCNT predicted maximum surface loading (Table 2). This increased sorption above the simulated surface adsorption capacity suggests that equilibrium was not reached within 24 h and sorption continued because of secondary interactions with higher activation energies (e.g., internal sorption sites, RDX–RDX interactions).

The initial loading of W onto nano-Al_2O_3 was 50% of the total loading measured at 21 d (Figure 3b). However, after a rapid initial increase during the initial 24 h, the system approached equilibrium, with maximum sorption occurring at 14 d and no further increase, indicating that the long-term (>24 h) sorption is small compared with the short-term interactions. Studies of other metals have found that increased loading after 24 h to 48 h can be significant. For example, Garnier et al. [50] found that long-term sorption (>48 h) accounted for anywhere from 5% to 25% of the total loading for various metals interacting with suspended matter in river water, similar to the 20% additional loading observed in the present study after 24 h. Since the total loading values are less than the surface coverage values predicted by the Langmuir isotherm model, the asymptotic approach to equilibrium is likely the result of high surface area diffusion limitations—such as interparticle diffusion, intrapore diffusion, and molecular sieving—as equilibrium between the adsorption sites and the WO_4^{2-} ions is reached. The high surface area of nano-Al_2O_3 (Table 1) supports this concept, suggesting a large number of potential surface sorption sites, including difficult-to-access pore spaces.

Desorption

Because RDX–MWCNT and W–nano-Al_2O_3 kinetic interactions indicated significant increases in sorption over time (Figure 3), desorption experiments were conducted to observe the strength and reversibility of munitions constituent adsorption onto the nanomaterials and to identify any hysteresis. To observe differences between short-term and long-term interactions, desorption was measured in parallel tests using samples that had experienced either 1 d or 21 d of initial sorption, respectively, prior to desorption tests.

On resuspending in clean MHRW, RDX-loaded MWCNT samples lost 20% (1 d) and 25% (21 d) of their RDX surface loading (Figure 4a). However, after this initial rinsing loss, the samples experienced very little (8%, 1 d) or no (21 d; Figure 3a) additional desorption during 14 d of mixing in clean MHRW. This indicates that a smaller fraction of the sorbed RDX is more loosely attached and therefore easily removed from the MWCNTs, while the remainder is much more strongly bound because it did not desorb even after vigorous mixing in clean MHRW over 14 d.

In addition to the above-mentioned n-π bonding, another possible mechanism for the strong initial adsorption is chemisorption, which is the result of a chemical reaction between the sorbent and sorbate leading to an irreversibly sorbed degradation product covalently attached to the MWCNT surface. This was previously shown to be a factor in regeneration studies using RDX and activated carbon [51,52], in which repeated sorption/desorption cycling results in irreversible binding because of $-NO_2$ electron transfer. However, this mechanism allows little additional sorption after the chemisorption and limits total sorption to a monolayer, after which all adsorption sites are filled. Furthermore, no RDX degradation byproducts were observed by HPLC analysis. Since we observed both increasing sorption with time in kinetic studies (Figure 3) and no significant degradation of RDX, we postulate that n-π electron donor–acceptor sorption was likely the dominant mechanism.

Because of the multiple sorption capacities seen in the present experiments, we believe the RDX and MWCNTs likely interact through multiple sorption mechanisms with different activation energies. We hypothesize that the rapid initial RDX–MWCNT sorption is a result of n-π electron polarization of the MWCNTs by the RDX molecules at the surface of the nanotubes [22] and that additional binding requires second-order interactions such as multilayer sorption or RDX–RDX interactions. Attempts to model the adsorption data using multilayer isotherm models were unsuccessful; therefore, we hypothesize that the majority of

the long-term sorption is governed by RDX–RDX interactions. Clustering of RDX molecules was previously shown to be substantial because of the presence of ions in solution [49]. It is possible that the polarization of the MWCNT–RDX system acts in a similar way, facilitating RDX clustering on the surface of the nanotubes that acts as a secondary adsorption mechanism.

The RDX loading of both the 1-d and 21-d samples after resuspending in clean MHRW was very close to the Langmuir-predicted value of 1.4 mg RDX/g MWCNT (Equation 1 with $C_e = 2$ mg/L RDX). This provides further evidence of a strong, initial surface sorption interaction between RDX and the MWCNTs, followed by a weaker additional sorption as a result of second-order interactions. Although the strong surface sorption will likely limit bioavailability, acting as an RDX sink, the reversible secondary interaction could potentially increase the bioavailability of RDX in the environment. The nanotubes could act as a carrier, transporting the RDX into close proximity to an organism through dermal contact or ingestion, where desorption of the loosely bound material could then increase availability for uptake [21,25,53]. More work is needed to explore this secondary interaction in detail and measure the extent and nature of the reversible portion of RDX sorption and its potential impact in environmental settings.

For W, the longer sorption period (21 d) resulted in increased sorption (1.9 mg W/g nano-Al_2O_3 compared with 0.9 mg W/g nano-Al_2O_3 for the 1-d sorption test; Figure 4b). Only 15% of the W adsorbed during the 21-d sample desorbed during the initial MHRW resuspension, whereas 33% of the W adsorbed by the 1-d samples was desorbed in this initial rinse. This indicates that increased sorption time increases not only the overall W sorption—as confirmed by the kinetic data—but also the sorption strength, because a smaller fraction of the W was rinsed off after a longer sorption. Furthermore, over the course of the 14-d desorption experiment, an additional 23% (21 d) or 50% (1 d) of the adsorbed W was desorbed. This shows a significant level of reversibility in W–nano-Al_2O_3 sorption and confirms that increased adsorption time produces stronger adsorption.

All samples showed some desorption (Figure 4), but none of the loadings were reduced by more than 50% after initial rinsing. Furthermore, even with vigorous mixing in clean water for 14 d, a significant portion (>30%) of munitions constituent remained attached to the nanomaterials in every case, indicating that some of the sorption is readily reversible, but a portion of the munitions constituent material is not easily removed from the nanomaterial surface. For these combinations of munitions constituent and nanomaterial, sorption interactions could significantly influence the fate and transport of munitions constituents in the environment.

Implications

Nanomaterials and munitions constituents are likely to be found together in the environment, especially in close proximity to military training or manufacturing facilities. Because co-occurrence of these materials is likely, understanding their interactions allows for more accurate predictions of bioavailability, fate, and ecological impact. Strong sorption of munitions constituents onto nanomaterials implies lower bioavailability and risk in the environment. It should be noted, however, that if the nanomaterials are themselves bioavailable, this could lead to a carrier effect in which the nanomaterials bring the munitions constituents into contact with susceptible organisms (e.g., filter-feeders), increasing bioavailability and bioaccumulation. This effect was previously demonstrated with fullerenes and nano-titanium dioxide as carrier materials [21,54,55]. Such increased bioavailability could be especially important when a significant fraction of the munitions constituent is loosely bound to the nanomaterial and could be released on contact with biological receptors. Follow-up investigations to the present study involve bioaccumulation experiments to determine the potential for these munitions constituent–nanomaterial interactions to reduce or enhance tissue residues and to determine the influence of water-quality parameters such as ionic strength, pH, and the concentration and type of natural organic matter, which could have a significant impact on these interactions.

Acknowledgment—Permission was granted by the Chief of Engineers to publish this material. This work was supported by the Army's Environmental Quality Technology Basic Research Program (Dr. E. Ferguson, Technical Director). The authors thank N.E. Harms and P. Chappell for their contributions to the sorption and desorption experiments and A. Harmon and C. Detzel for characterization assistance.

REFERENCES

1. Ramaswamy Alba L, Kaste P, Miziolek Andrzej W, Homan B, Trevino S, O'Keefe Michael A. 2005. Nanoenergetics Weaponization and Characterization Technologies. In Miziolek AW, Karna S, Mauro JM, Vaia RJ, eds, *Defense Applications of Nanomaterials*, Vol 891. ACS Symposium Series. American Chemical Society, Washington, DC, pp 180–197.
2. Yarrington CD, Son SF, Foley TJ, Obrey SJ, Pacheco AN. 2011. Nano aluminum energetics: The effect of synthesis method on morphology and combustion performance. *Propellants, Explosives, Pyrotechnics* 36:551–557.
3. Poda AR, Moser RD, Cuddy MF, Doorenbos Z, Lafferty BJ, Weiss CA, Harmon A, Chappell MA, Steevens JA. 2013. Nano-aluminum thermite formulations: Characterizing the fate properties of a nanotechnology during use. *Journal of Nanomaterials & Molecular Nanotechnology.* DOI: 10.4172/2324-8777.1000105
4. Atkinson KR, Hawkins SC, Huynh C, Skourtis C, Dai J, Zhang M, Fang S, Zakhidov AA, Lee SB, Aliev AE, Williams CD, Baughman RH. 2007. Multifunctional carbon nanotube yarns and transparent sheets: Fabrication, properties, and applications. *Physica B* 394:339–343.
5. Geim AK. 2009. Graphene: Status and prospects. *Science* 324:1530–1534.
6. Jornet JM, Akyildiz IF. 2011. Channel modeling and capacity analysis for electromagnetic wireless nanonetworks in the terahertz band. *IEEE Transactions on Wireless Communications* 10:3211–3221.
7. Qu X, Brame J, Li Q, Alvarez PJJ. 2012. Nanotechnology for a safe and sustainable water supply: Enabling integrated water treatment and reuse. *Accounts of Chemical Research* 46:834–843.
8. Masciangioli T, Zhang W-X. 2003. Environmental technologies at the nanoscale. *Environ Sci Technol* 37:102A–108A.
9. Iorio M, Pan B, Capasso R, Xing B. 2008. Sorption of phenanthrene by dissolved organic matter and its complex with aluminum oxide nanoparticles. *Environ Pollut* 156:1021–1029.
10. Yang K, Zhu L, Xing B. 2010. Sorption of phenanthrene by nanosized alumina coated with sequentially extracted humic acids. *Environ Sci Pollut Res* 17:410–419.
11. Szecsody JE, Girvin DC, Devary BJ, Campbell JA. 2004. Sorption and oxic degradation of the explosive CL-20 during transport in subsurface sediments. *Chemosphere* 56:593–610.
12. Bednar AJ, Jones WT, Boyd RE, Ringelberg DB, Larson SL. 2008. Geochemical parameters influencing tungsten mobility in soils. *J Environ Qual* 37:229–233.
13. Pacheco S, Rodríguez R. 2001. Adsorption properties of metal ions using alumina nano-particles in aqueous and alcoholic solutions. *J Sol-Gel Sci Tech* 20:263–273.
14. Wang X, Lu J, Xing B. 2008. Sorption of organic contaminants by carbon nanotubes: Influence of adsorbed organic matter. *Environ Sci Technol* 42:3207–3212.
15. Long RQ, Yang RT. 2001. Carbon nanotubes as superior sorbent for dioxin removal. *J Am Chem Soc* 123:2058–2059.
16. Pan B, Xing B. 2008. Adsorption mechanisms of organic chemicals on carbon nanotubes. *Environ Sci Technol* 42:9005–9013.
17. Li H, Pan L, Zhang Y, Sun Z. 2009. Ferric ion adsorption and electrodesorption by carbon nanotubes and nanofibres films. *Water Sci Technol* 59:1657–1663.

18. Salam MA, Mohamed RM. 2013. Removal of antimony (III) by multi-walled carbon nanotubes from model solution and environmental samples. *Chem Eng Res Des* 91:1352–1360.
19. Tawabini B, Al-Khaldi S, Atieh M, Khaled M. 2010. Removal of mercury from water by multi-walled carbon nanotubes. *Water Sci Technol* 61:591–598.
20. Ghaedi M, Montazerozohori M, Nazari E, Nejabat R. 2013. Functionalization of multiwalled carbon nanotubes for the solid-phase extraction of silver, cadmium, palladium, zinc, manganese and copper by flame atomic absorption spectrometry. *Hum Exp Toxicol* 32:687–697.
21. Zhang L, Wang L, Zhang P, Kan AT, Chen W, Tomson MB. 2011. Facilitated transport of 2,2′,5,5′-polychlorinated biphenyl and phenanthrene by fullerene nanoparticles through sandy soil columns. *Environ Sci Technol* 45:1341–1348.
22. Chen W, Duan L, Zhu D. 2007. Adsorption of polar and nonpolar organic chemicals to carbon nanotubes. *Environ Sci Technol* 41:8295–8300.
23. Mylvaganam K, Zhang LC. 2007. Ballistic resistance capacity of carbon nanotubes. *Nanotechnology* 18:475701.
24. Yang Y, Gupta MC, Dudley KL, Lawrence RW. 2005. A comparative study of EMI shielding properties of carbon nanofiber and multi-walled carbon nanotube filled polymer composites. *J Nanosci Nanotechnol* 5:927–931.
25. Stanley JK, Coleman JG, Weiss CA, Steevens JA. 2010. Sediment toxicity and bioaccumulation of nano and micron-sized aluminum oxide. *Environ Toxicol Chem* 29:422–429.
26. Coleman JG, Johnson DR, Stanley JK, Bednar AJ, Weiss CA, Boyd RE, Steevens JA. 2010. Assessing the fate and effects of nano aluminum oxide in the terrestrial earthworm, *Eisenia fetida*. *Environ Toxicol Chem* 29:1575–1580.
27. Chappell MA, George AJ, Dontsova KM, Porter BE, Price CL, Zhou P, Morikawa E, Kennedy AJ, Steevens JA. 2009. Surfactive stabilization of multi-walled carbon nanotube dispersions with dissolved humic substances. *Environ Pollut* 157:1081–1087.
28. Kennedy AJ, Hull MS, Steevens JA, Dontsova KM, Chappell MA, Gunter JC, Weiss CA. 2008. Factors influencing the partitioning and toxicity of nanotubes in the aquatic environment. *Environ Toxicol Chem* 27:1932–1941.
29. Kennedy AJ, Gunter JC, Chappell MA, Goss JD, Hull MS, Kirgan RA, Steevens JA. 2009. Influence of nanotube preparation in aquatic bioassays. *Environ Toxicol Chem* 28:1930–1938.
30. US Environmental Protection Agency. 2002. *Methods for Measuring the Acute Toxicity of Effluents and Receiving Waters to Freshwater and Marine Organisms*. 5th ed. Washington, DC.
31. Schwarzenbach R, Gschwend P, Imboden D. 2003. *Environmental Organic Chemistry*. 2nd ed. John Wiley and Sons, Hoboken, NJ, USA.
32. Pennington JC, Brannon JM. 2002. Environmental fate of explosives. *Thermochimica Acta* 384:163–172.
33. Hyung H, Fortner JD, Hughes JB, Kim J-H. 2006. Natural organic matter stabilizes carbon nanotubes in the aqueous phase. *Environ Sci Technol* 41:179–184.
34. Dermatas D, Braida W, Christodoulatos C, Strigul N, Panikov N, Los M, Larson S. 2004. Solubility, sorption, and soil respiration effects of tungsten and tungsten alloys. *Environmental Forensics* 5:5–13.
35. Wang L, Zhu D, Duan L, Chen W. 2010. Adsorption of single-ringed N- and S-heterocyclic aromatics on carbon nanotubes. *Carbon* 48:3906–3915.
36. Sharma P, Mayes MA, Tang G. 2013. Role of soil organic carbon and colloids in sorption and transport of TNT, RDX and HMX in training range soils. *Chemosphere* 92:993–1000.
37. Price CB, Brannon JM, Yost SL, Hayes CA. 2001. Adsorption and transformation of RDX in low-carbon aquifer soils. ERDC/EL-TR-01-19. US Army Corps of Engineers, Washington, DC.
38. Shen X-E, Shan X-Q, Dong D-M, Hua X-Y, Owens G. 2009. Kinetics and thermodynamics of sorption of nitroaromatic compounds to as-grown and oxidized multiwalled carbon nanotubes. *Journal of Colloid and Interface Science* 330:1–8.
39. Coughlin RW, Ezra FS. 1968. Role of surface acidity in the adsorption of organic pollutants on the surface of carbon. *Environ Sci Technol* 2:291–297.
40. Kaneko Y, Abe M, Ogino K. 1989. Adsorption characteristics of organic compounds dissolved in water on surface-improved activated carbon fibres. *Colloids and Surfaces* 37:211–222.
41. Li L, Quinlivan PA, Knappe DRU. 2002. Effects of activated carbon surface chemistry and pore structure on the adsorption of organic contaminants from aqueous solution. *Carbon* 40:2085–2100.
42. Franz M, Arafat HA, Pinto NG. 2000. Effect of chemical surface heterogeneity on the adsorption mechanism of dissolved aromatics on activated carbon. *Carbon* 38:1807–1819.
43. Khalid M, Mushtaq A, Iqbal MZ. 2001. Sorption of tungsten(VI) and rhenium(VII) on various ion-exchange materials. *Sep Sci Technol* 36:283–294.
44. Vissenberg MJ, Joosten LJM, Heffels MMEH, van Welsenes AJ, de Beer VHJ, van Santen RA. 2000. Tungstate versus molybdate adsorption on oxidic surfaces: A chemical approach. *J Phys Chem B* 104:8456–8461.
45. Karakonstantis L, Kordulis C, Lycourghiotis A. 1992. Mechanism of adsorption of tungstates on the interface of gamma-alumina/electrolyte solutions. *Langmuir* 8:1318–1324.
46. Chakravarty R, Dash A. 2013. Nano structured metal oxides as potential sorbents for 188W/188Re generator: A comparative study. *Sep Sci Technol* 48:607–616.
47. Pignatello JJ, Xing B. 1995. Mechanisms of slow sorption of organic chemicals to natural particles. *Environ Sci Technol* 30:1–11.
48. Hou PX, Bai S, Yang QH, Liu C, Cheng HM. 2002. Multi-step purification of carbon nanotubes. *Carbon* 40:81–85.
49. Gapeev A, Sigman M, Yinon J. 2003. Liquid chromatography/mass spectrometric analysis of explosives: RDX adduct ions. *Rapid Commun Mass Spectrom* 17:943–948.
50. Garnier J-M, Ciffroy P, Benyahya L. 2006. Implications of short and long term (30 days) sorption on the desorption kinetic of trace metals (Cd, Zn, Co, Mn, Fe, Ag, Cs) associated with river suspended matter. *Sci Total Environ* 366:350–360.
51. Haberman J, Castorina TC. 1982. Charcoal regeneration—Part III. Mechanism of RDX adsorption. Technical report. ARLCD-TR-82002. US Army Armament Research and Development Command, Dover, NJ.
52. Lee CKM, Stenstrom MK. 1996. Competitive adsorption of cyclotrimethylenetrinitramine (RDX) and cyclotetramethylenetetranitramine (HMX). Report ENG 96-152. School of Engineering and Applied Science, University of California, Los Angeles, USA.
53. Yu Z-G, Wang W-X. 2013. Influences of ambient carbon nanotubes on toxic metals accumulation in *Daphnia magna*. *Water Res* 47:4179–4187.
54. Zhang X, Sun H, Zhang Z, Niu Q, Chen Y, Crittenden JC. 2007. Enhanced bioaccumulation of cadmium in carp in the presence of titanium dioxide nanoparticles. *Chemosphere* 67:160–166.
55. Sun H, Zhang X, Zhang Z, Chen Y, Crittenden JC. 2009. Influence of titanium dioxide nanoparticles on speciation and bioavailability of arsenite. *Environ Pollut* 157:1165–1170.